Acta Cryst. (1985). B41, 281–292

On the Nature of the 'Short-Range Order' in $1\frac{1}{2}0$ Alloys

BY G. VAN TENDELOO AND S. AMELINCKX*

RUCA, University of Antwerp, Groenenborgerlaan 171, *B2020-Antwerpen, Belgium*

AND D. DE FONTAINE

Department of Materials Science and Mineral Engineering, University of California, Berkeley, CA 94720, *USA*

(*Received* 27 *June* 1984; *accepted* 8 *March* 1985)

Abstract

High-resolution electron-microscope images of the $\langle 1\frac{1}{2}0\rangle$ special-point short-range-ordering alloys Ni_4Mo, Au_4Cr, Au_4V and Au_4Fe are compared, and the extent to which optical diffractograms from local regions of such micrographs can be interpreted is discussed. For Au_4Cr and Ni_4Mo, the observed state or order can be interpreted as being due to the presence of microdomains of the $D0_{22}$ structure and elements of the $D1_a$ structure, extending sometimes several unit cells along the **c** direction, but being quite often only one or a small number of unit cells wide. For Au_4V and Au_4Fe, the observed diffuse intensity is probably too weak to allow decisive conclusions. It is argued that the 'microdomain' model and the 'concentration-wave' model are two descriptions of the same physical reality which are revealed by different imaging modes. A reinterpretation of some results obtained by X-ray diffraction on Ni_4Mo by Chakravarti, Starke, Sparks & Williams [*J. Phys. Chem. Solids* (1974), **35**, 1317–1326] confirm the proposed model.

1. Introduction

It is expected that short-range order (SRO) in alloys will manifest itself by broad diffuse intensity maxima in reciprocal space in the vicinity of points where the second derivative F'' of the free energy will have a minimum value. Of particular interest are those points at which extrema of F'' must exist for symmetry reasons alone: these are so-called *special points* (SP) which satisfy the Lifshitz criterion requiring that two or more symmetry elements intersect at a point (de Fontaine, 1979). The relative local site occupation of the constituents of such alloys in this state can differ markedly from those characteristic of long-range order (LRO) at the same compositions, however. Indeed, the LRO state results from the minimization of the internal energy, whereas the SRO state results from the minimization of F''. The distinction between LRO and SRO is particularly apparent in solid solutions belonging to the $1\frac{1}{2}0$ family, *i.e.* for which F'' has a minimum at that particular SP. That is because, for those systems, the corresponding LRO states have superlattice peaks at positions other than the $1\frac{1}{2}0$ SP. Rather than attempting to study SRO directly at temperatures above ordering, it is simpler, from an experimental viewpoint, to quench such alloys rapidly to low temperatures so as to avoid nucleation of the equilibrium LRO state. In so doing, the *ordering spinodal* may be crossed in a temperature range where atomic mobility is still appreciable, thereby leading to amplification of the associated SP concentration wave (de Fontaine, 1975).

It is tempting to try to interpret these SRO effects in direct (or 'real') space, noting that the SRO state should probably be a prefiguration of the LRO state. Ruedl, Delavignette & Amelinckx (1968) were the first to observe 'bright speckles' in dark-field transmission electron microscopy, and interpreted these as ordered microdomains having the LRO structure. Although a random distribution of very small microdomains belonging to all possible orientation variants may produce diffuse maxima at the $1\frac{1}{2}0$ positions, it is now thought that the size of the observed speckles was presumably too large to allow their interpretation as images of single microdomains. For this system, Okamoto & Thomas (1971) therefore proposed a more elaborate microdomain interpretation based upon the presence of non-conservative antiphase boundaries (APB's) along the (420) f.c.c. planes in the ordered structure.

After crossing the spinodal, a pure SRO fluctuation state surely cannot be maintained, and the system will spontaneously begin to evolve towards the expected LRO state along paths which are very difficult to predict theoretically as they will evolve non-linearities in the free-energy function. Hence, an interpretation based on an intermediate state between SRO and LRO is perhaps to be preferred. Such an interpreta-

* Also at: SCK/CEN, B 2400-Mol, Belgium.

0108-7681/85/050281-12$01.50

tion was suggested by De Ridder, Van Tendeloo, Van Dyck & Amelinckx (1976) who characterized the state of order by clusters of a specific type, the type of cluster(s) being determined from the geometry of the diffuse intensity pattern.

In the present paper, we shall re-examine, by means of high-resolution electron microscopy, SRO in various $1\frac{1}{2}0$ family alloys, namely Ni_4Mo, Au_4V, Au_4Cr and Au_4Fe, and we shall try to determine what may be the most appropriate qualitative description.

It will be found that the two competing concepts 'concentration waves' (de Fontaine, 1975) *vs* 'microdomains' (Ruedl *et al.*, 1968) are in fact two aspects of the same physical reality or two languages to describe the same phenomenon. A wave with a wavelength equal to interatomic distances in a discrete medium, consisting of atoms on a lattice, can in fact only be materialized as a configuration of atoms on an appropriate geometrical pattern. It will be shown furthermore that the present results are also compatible with the conclusions of the cluster model as described by De Ridder, Van Tendeloo, Van Dyck & Amelinckx (1976).

2. Experimental evidence; previous observations

An interesting point is that while all three materials, in the as-quenched state, scatter electrons to the $1\frac{1}{2}0$ reciprocal-lattice positions, the diffuse scattering shows characteristic differences between the different alloys which should be of help in choosing descriptions for the SRO state. Diffraction patterns obtained along [001] for the four alloys are shown in Fig. 1. The first point to note is that we find the $1\frac{1}{2}0$ scattering most intense for Ni_4Mo and least intense for Au_4Fe. Given the different atomic scattering factors involved, this is the inverse of what would be expected for the same degree of order. We can also see from Fig. 1 that while the $1\frac{1}{2}0$ scattering is relatively symmetrically distributed about this position for Ni_4Mo, it tends to be somewhat elongated towards the f.c.c. matrix reflections for Au_4V or for Au_4Fe but in each case in a somewhat different way. Whereas for Au_4Fe this linking intensity tends to be curved in towards ⟨100⟩ positions, the curvature has the opposite tendency for Au_4V. During this discussion, it is assumed that these observations reflect the SRO state and that no nuclei for LRO have formed. The conditions for retaining the SRO state are different for the alloys used. Au_4Fe can be aged for several days at temperatures in the range 720–920 K without showing any development of LRO. For Ni_4Mo, a fast quench rate is required to retain the SRO state. Other alloys such as Au_4Mn (another member of the $1\frac{1}{2}0$ family) can only be retained in the SRO state by splat cooling. The usual fast water quench produces a long-range-ordered transition state (Van Tendeloo, De Ridder & Amelinckx, 1978).

The development of long-range order in Ni_4Mo has been studied in detail by electron diffraction and electron microscopy (Ruedl *et al.*, 1968; Okamoto & Thomas, 1971; Van Tendeloo, 1976; De Ridder, Van Tendeloo & Amelinckx, 1976; Chevalier & Stobbs, 1979; Thomas & Sinclair, 1977; Van Tendeloo & Amelinckx, 1981*b*). On slight annealing, diffuse 'circles' are formed in reciprocal space just outside the $1\frac{1}{2}0$ positions, *i.e.* different from the diffuse intensity observed for Au_4V or Au_4Fe (Fig. 1*c*,*d*). The ordering process in Au_4Cr was studied by Dutkiewicz & Thomas (1975). Using electron diffraction and lattice imaging, they concluded that the transformation from SRO to LRO occurs with the formation of a transitional ordered phase (similar to $D0_{22}$) which can be described in terms of composition modulations along [001] (with a wavelength equal to the *c*-parameter of the $D0_{22}$ structure). Au_4V has only been studied to a limited extent using electron diffraction by De Ridder, Van Tendeloo, Van Dyck & Amelinckx (1976), but a much more thorough study has been performed using X-ray diffraction by Furnrohr (1976). For Au_4Fe, X-ray diffraction studies by Dartyge, Bouchiat & Monod (1982) have shown the existence of diffuse intensity streaks with maxima at the $1\frac{1}{2}0$. The present observations are the first ones obtained by electron diffraction (Stobbs, 1983).

Until now, the most convincing technique to prove (or disprove) the presence of microdomains was to make dark-field images using the $1\frac{1}{2}0$ diffuse intensity in the manner of Ruedl *et al.* (1968); see *e.g.* Chevalier (1980). When doing so, for the four alloys, one observes speckles of the order of 0·5–1 nm depending

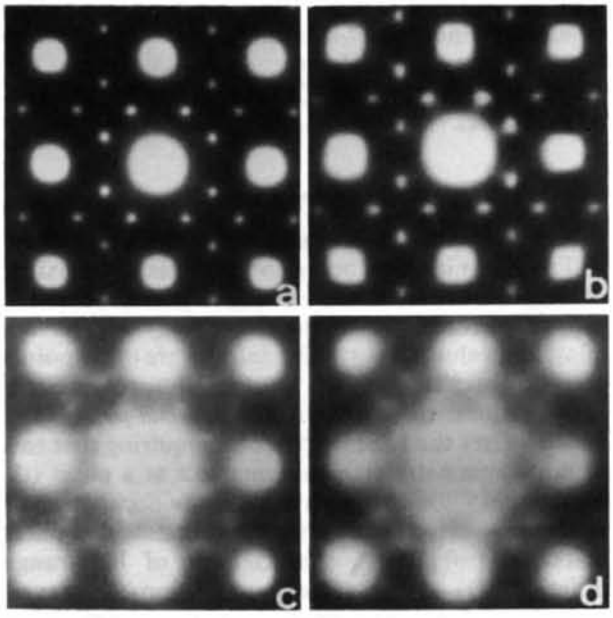

Fig. 1. Electron diffraction patterns along [001] for four different alloys showing diffuse intensity around $1\frac{1}{2}0$ positions. (*a*) Ni_4Mo; (*b*) Au_4Cr; (*c*) Au_4V; (*d*) Au_4Fe.

on the degree of order. The interpretation, however, is not clear since the size of the speckles is such that they could be produced by microdomains as well as by the presence of the objective aperture. Moreover, it has been observed in the case of Ni_4Mo that the speckles grow more intense and larger during long observations (Van Tendeloo, 1980). This may be due to contamination of the specimen surface and/or formation of a Mo_2C film at the surface which, in dark field, also produces speckles of the same type as the possible Ni_4Mo microdomains (Kesternich, Carpenter & Kenik, 1982). Possibly, the early dark-field observations by Ruedl *et al.* (1968) showing larger (2–3 nm) dark-field speckles have to be attributed, at least in part, to contamination in the microscope.

3. Experimental evidence: new observations and their interpretation

3.1. *Reciprocal space: diffraction patterns*

The diffraction vectors corresponding to the positions of the SRO spots are $\mathbf{k}_1=(1/a)[1\frac{1}{2}0]$; $\mathbf{k}_2=(1/a)[\frac{1}{2}10]$ and the crystallographically related ones $\pm\mathbf{k}_1$, $\pm\mathbf{k}_2$; $\pm\mathbf{k}_3$ and $\pm\mathbf{k}_4$ shown in Fig. 2(*a*), where a is the lattice parameter of the basic f.c.c. structure. These vectors are also the first-order diffraction vectors corresponding to the {101}-type planes of the $D0_{22}$ structure based on the same cubic lattice.

It is therefore suggestive to use atom configurations derived from the $D0_{22}$ structure as the ingredients of a possible model of the SRO state. The $D0_{22}$ as well as the $D1_a$ structure are represented schematically in Fig. 3. The first-order spots 101 of the two variants of the $D0_{22}$ structure, which have their c axis perpendicular to the viewing direction, lead to the four observed SRO diffraction spots (Fig. 2*a*,*b*). The second-order spots, 202, which are present in the $D0_{22}$ structure, are absent in the diffraction pattern of the SRO state. This suggests that the disorder affects the d_{202} spacings in such a way that the second-order spots are suppressed. The insertion of a slab of $D1_a$-type atom configurations (Fig. 4) causes a shift of $\frac{1}{4}$ of the {101} planes, but a shift of $\frac{1}{2}$ of the {202} planes (represented as broken lines in Fig. 4). The second-order spots will thus be much more suppressed by the introduction of this type of defect than the first-order spot.

During the first stages of LRO ordering, one observes in the diffraction pattern that intensity is 'transferred' from the $1\frac{1}{2}0$-type spots to the $\frac{4}{5}\frac{2}{5}0$ spots (Fig. 2*c*). This corresponds to a reduction in length of the diffraction vector, without a change in its direction.

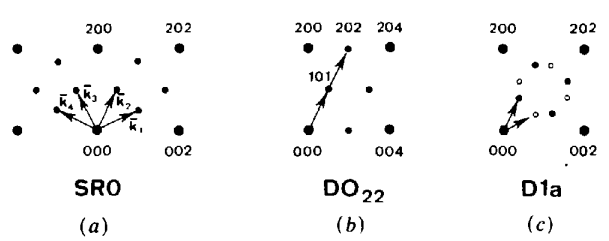

Fig. 2. Schematic representation of three diffraction patterns relevant for the understanding of the SRO state and the evolution towards LRO in $1\frac{1}{2}0$ alloys. (*a*) A cubic section of the SRO state with only reflections at $1\frac{1}{2}0$ positions. (*b*) A [010] section of the tetragonal $D0_{22}$ structure. (*c*) A [001] section of the tetragonal $D1_a$ structure. Superstructure reflections of two variants, having a common c axis, are indicated by small open and closed dots.

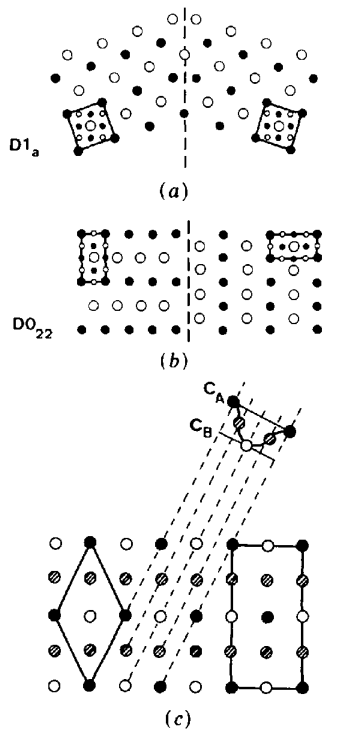

Fig. 3. Representation of (*a*) the $D1_a$ and (*b*) the $D0_{22}$ structures projected along one of the axes of the basic f.c.c. structure. Different variants are represented. In (*c*) an 'average projected $D0_{22}$' structure is represented. Black dots represent A atoms, open circles are B atoms and hatched circles represent a mixture of A and B atoms (projected along the viewing direction). The A atoms are still in a $D0_{22}$ configuration but a concentration modulation is obvious along the (420) f.c.c. $\equiv$ (101)$D0_{22}$ planes (broken lines) (after de Fontaine, 1975).

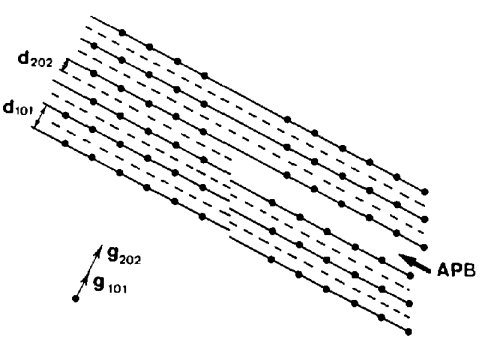

Fig. 4. Schematic representation of the $D0_{22}$ structure as projected along [010]; only the minority atoms are indicated. The introduction of a slab of $D1_a$ configuration causes a shift of $\frac{1}{4}$ of the (101) planes and of $\frac{1}{2}$ of the (202) planes.

In direct space, this means an increase in average spacing, *i.e.* that possibly slabs of $D1_a$ structure are introduced between the {101} planes of $D0_{22}$ structure (Fig. 4). Depending on the proportion of $D0_{22}$ and $D1_a$ slabs, the average spacing will vary, and hence also the position of the intensity maximum will shift from the SRO position to the $D1_a$ position. The 'wings' of diffuse intensity, connecting the $D1_a$ spots with the SRO spots, can be attributed to disorder in the arrangement of $D0_{22}$ and $D1_a$ slabs in the two families of {101} planes of a given variant of $D0_{22}$.

Since the three orientation variants of the $D0_{22}$ structure are *a priori* equally probable, one would expect to find in the diffraction pattern evidence also for the variant which has its c axis parallel to the viewing direction. As yet, there is no reference in the literature to the presence of the 110 reflection (at the center of the square of $1\frac{1}{2}0$ reflections), which would indicate the presence of this third $D0_{22}$ variant. In an attempt to find such evidence, we have deliberately overexposed the diffraction pattern of a small selected area of Au_4Cr, which was briefly annealed at 543 K, such that the SRO spots remain prominently present; it is reproduced in Fig. 5. It is quite clear that a surprisingly sharp 110 reflection is present. The second-order reflections of the type 120, on the other hand, are not observed. Tilting experiments show that the 110 reflection is streaked along the viewing direction, but very sharp along the lateral directions. This seems to indicate that the c domains are small along the viewing direction and larger along the lateral dimensions. Along the [100] direction, there is apparently some planar disorder. Moreover, the diffracted amplitudes, due to the sets of {110} planes in this different translation variants, are either in phase or in antiphase. This means that the d_{110} spacing in c domains is well defined even in the presence of domain fragmentation, and the 110 reflection consequently remains sharp. If all translation variants are present in equal volumes of the crystal, the resultant amplitude will be zero; only if the selected area contains unequal volumes of the different translation variants will a non-vanishing 110 reflection result. This is presumably the reason why the 110 reflection is often weak and sometimes absent, and remained unobserved until now.

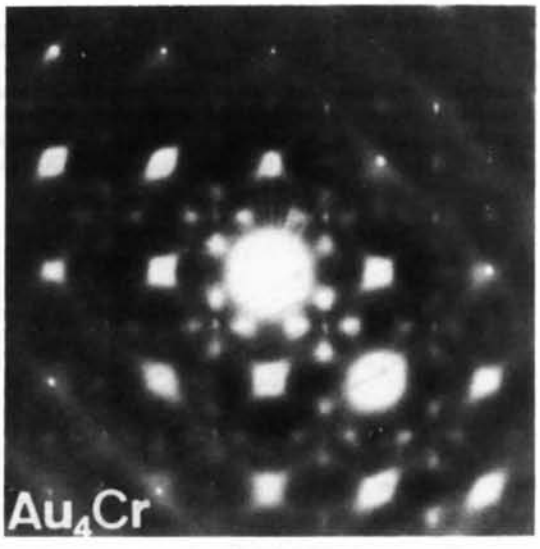

Fig. 5. A [001] diffraction pattern of Au_4Cr quenched from 823 K and annealed for 3 h at 543 K. Note the presence of the weak 110 reflections at the center of the square of four $1\frac{1}{2}0$ spots.

3.2. *Direct space*

3.2.1. *High-resolution images; dot patterns.* Recent improvements in the resolution of modern electron microscopes have led us to re-examine whether or not useful information can be obtained on the structure of the SRO state in $1\frac{1}{2}0$ alloys, using axial high-resolution observations. Similar observations in Cu_3Pd have led to positive conclusions and have illustrated the importance of choosing the right objective diaphragm. Images made using a large aperture (including f.c.c. reflections up to 220) show lattice details, but obscure the ordering effects, while images obtained with an aperture just excluding the first 200 f.c.c. reflections show the ordered microdomains very clearly (Van Tendeloo & Amelinckx, 1983).

Axial-illumination high-resolution images using a large objective aperture including basic $200_{\text{f.c.c.}}$ and $220_{\text{f.c.c.}}$ reflections mainly show a regular square arrangement of bright dots separated by $\sim 0{\cdot}2$ nm ($=d_{200}$) and provide little information about possible ordering.

However, the bright-field image, obtained using a smaller objective diaphragm only including the central beam and the nearest eight SRO reflections (Figs. 6, 7), rejecting the redundant information from the f.c.c. lattice, shows a reduced resolution but clearly exhibits bright dots aligned in small clusters (encircled areas). In almost all clusters, the arrangement characteristic of one of the three $D0_{22}$ variants can be recognized. The borders of such clusters (where the periodicity breaks down) often consist of an arrangement of the $D1_a$ type.

The optical diffraction patterns of the high-resolution images under the two imaging modes are shown as insets in Figs. 6 and 7. The diffuse $1\frac{1}{2}0$ intensity is quite visible, indicating that information on the SRO state is recorded in the HREM pictures. When Au_4Cr is annealed for 3 h at 543 K, no changes are observed in the electron diffraction pattern apart from the appearance of an occasional weak 110 reflection. However, on the high-resolution image, using a limited aperture (Fig. 7), the effect of ordering is observed. The number of bright (or dark) dots forming a coherent microdomain is larger than in the as-quenched state observed in Fig. 6.

Very similar observations are made for Ni_4Mo (Fig. 8*a*,*b*). Again, we recognize limited areas where square or triangular arrangements of bright dots are observed in a configuration and spacing such that they resemble the projected minority-atom configurations in $D0_{22}$ or $D1_a$ structure.

For Au_4V and Au_4Fe, however, where the diffuse intensity is remarkably weaker, no clear cluster or microdomain formation has been observed in any of the high-resolution images. Optical diffraction patterns from the area having an intermediate thickness show a very weak and hardly interpretable diffuse intensity (Stobbs, 1983).

We shall now examine the direct-space evidence in relation to the diffraction patterns. In this respect, it is of interest to compare the annealing behavior of Au_4Mn, Au_4Cr and Ni_4Mo. Fully ordered Au_4Mn has the $D1_a$ structure; however, after a mild quench, this alloy exhibits a structure consisting of parallellogram-shaped islands of $D0_{22}$ structure of varying size (Van Tendeloo, De Ridder & Amelinckx, 1978) separated by antiphase boundaries containing structural elements of the $D1_a$ phase. In stoichiometric Au_4Mn this constitutes a metastable transition structure which disappears on annealing; in non-stoichiometric alloys $Au_{4-x}Mn$ this structure is stable and can be observed in symbiosis with the $D1_a$ structure and with a one- and two-dimensional long-period superstructure of the latter (Van Tendeloo & Amelinckx, 1981*a*). It is thus not unrealistic to assume that in

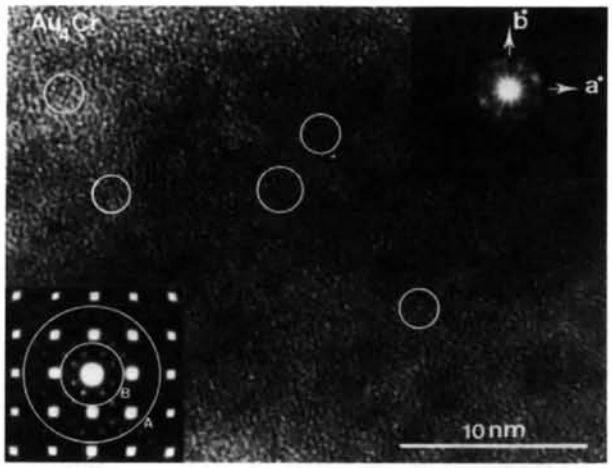

Fig. 6. High-resolution image of Au_4Cr, quenched from above T_c. Only the central beam and the nearest SRO reflections are used to produce the image (aperture *B* in the lower inset). The optical diffraction pattern (upper right inset) exhibits the diffuse maxima at $1\frac{1}{2}0$ positions.

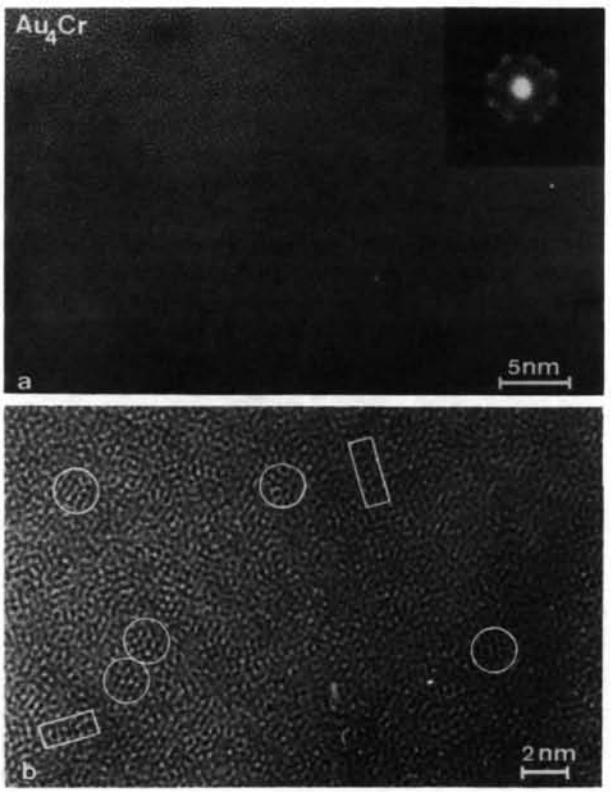

Fig. 7. A [001] image of Au_4Cr under the same conditions as in Fig. 6, but annealed for 3 h at 543 K. The number as well as the size of the ordered domains have increased although the diffraction pattern is still the same. Note the microdomains (or clusters) in the encircled areas. (*a*) Lower magnification; (*b*) high magnification.

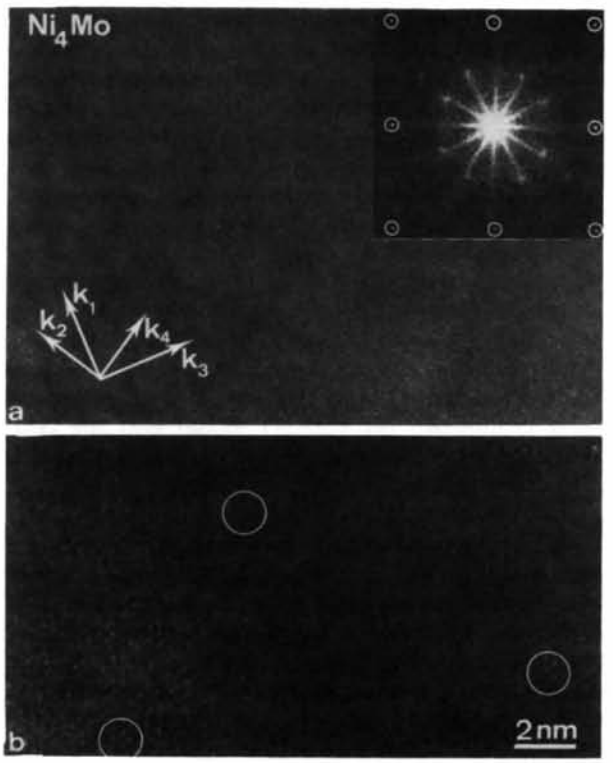

Fig. 8. A [001] high-resolution image of Ni_4Mo using a limited objective aperture similar to the one used to obtain Figs. 6 or 7. (*a*) Low magnification; (*b*) higher magnification. The optical diffraction pattern is reproduced as an inset.

quenched Ni_4Mo a similar $D0_{22}$-based type 'texture' occurs as in Au_4Mn. This texture would only appear in the embryonic stage, *i.e.* as very small microdomains, which, on further annealing at sufficiently high temperature, but still below the critical temperature for $D1_a$ ordering, would not grow very much, but develop into the $D1_a$ structure instead. The SRO state of Ni_4Mo would thus be derived in the first place from structural elements of $D0_{22}$-type configuration of the minority atoms (A atoms). Since under suitable imaging conditions a bright (or dark) dot has to be associated with a projected column of atoms, an 'average $D0_{22}$' structure as proposed by de Fontaine (1975) cannot be excluded (see Fig. 3*c*). This structure is an average structure, because one introduces 'grey atoms', *i.e.* a mixture along the viewing direction of A and B atoms. Of course, on an atomic scale, grey atoms do not exist (they are either A or B), but HREM only images a projected structure where small composition differences between neighboring columns cannot be detected. In Figs. 6, 7 and 8, we are imaging the minority-atom configurations but no decisive conclusions can be drawn about the exact occupation of the other atom columns. Pure B columns would be impossible to discern from B columns containing a number of A atoms as well. Below, we will continue talking about $D0_{22}$, keeping in mind that a concentration-wave type $D0_{22}$ arrangement (as in Fig. 3*c*) would be possible as well.

When viewing the photographs of Au_4Cr or Ni_4Mo at grazing incidence (*e.g.* in Fig. 8 along the indicated arrows), patches containing slightly wavy rows of somewhat brighter dots can be observed along the four directions indicated by arrows $\mathbf{k}_1$, $\mathbf{k}_2$, $\mathbf{k}_3$ and $\mathbf{k}_4$ in Fig. 8 and which are perpendicular to the vectors $\mathbf{k}_1$, $\mathbf{k}_2$, $\mathbf{k}_3$ and $\mathbf{k}_4$ in Fig. 2(*a*); their spacing is roughly $d_{101}(D0_{22})$. These rows can be considered as images of the 'concentration' waves that result from 'spinodal ordering'. Their direction and spacing suggest that the underlying structure would be the $D0_{22}$ structure. The bright dots, representing the cluster configurations, are situated on the observed rows or waves; the microdomain (or cluster) model and the concentration-wave model are in this respect two aspects of the same phenomenon.

3.2.2. *Dark-field images in* $1\frac{1}{2}0$ *spots.* In order to make the link with the original observations, using the diffraction contrast mode (Ruedl *et al.*, 1968; Okamoto & Thomas, 1971; Stobbs & Chevalier, 1978), which started the controversy on the nature of the $1\frac{1}{2}0$ state in Ni_4Mo and in structurally similar alloys, we have produced dark-field images in single $1\frac{1}{2}0$ spots in Au_4Cr (Fig. 9). As in the original observations in Ni_4Mo, we found also in this case the same type of small bright patches with irregular shapes, but now with better defined boundaries, and hence providing the possibility of obtaining a better estimate of their sizes than was possible hitherto. It was verified that very similar configurations of bright patches are found when using diffraction vectors such as $\mathbf{k}_1$ and $\mathbf{k}_4$ (Fig. 9*a*, *b*) belonging to two different variants of $D0_{22}$, both having their c axis perpendicular to the viewing direction.

The visibility and shape of the microdomains depend on the exact foil orientation. Therefore, there are slight differences in the images of Fig. 9(*a*) and Fig. 9(*c*). These photographs were made in the four SRO reflections in succession; at the end, the first SRO reflection was used once again in order to check the reproducibility and to rule out orientation changes during these operations. The dark dislocation image in Fig. 9 is a convenient reference mark. The size distribution of the bright patches is in qualitative agreement with that of the images of microdomains in the high-resolution images.

We conclude from this that the majority of the observed bright patches are presumably produced by microdomains of $D0_{22}$-type structure of a sufficient size. The dark areas are presumably due to other variants than those reflecting in the considered spot, or to regions where the coherency is not good enough to produce a reasonably sharp intensity maximum in the $1\frac{1}{2}0$ direction.

Whereas in the original paper of Ruedl *et al.* (1968) the bright patches were attributed to different variants of the $D1_a$ structure, it now seems more logical that different $D0_{22}$ variants are mainly responsible for their presence.

3.3. *Optical simulations*

In order to test the proposed models, it is convenient to construct optical gratings representing the

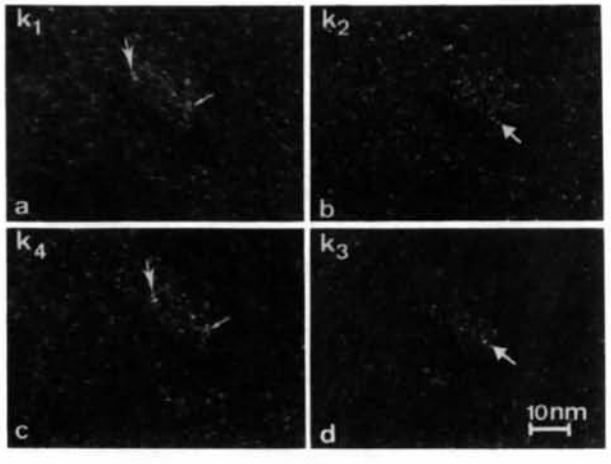

Fig. 9. Four dark-field images made in four different SRO reflections in Au_4Cr. The indicated vectors $\mathbf{k}_1$ refer to the schematic pattern of Fig. 2(*a*). Note that large similarities can be found between (*a*) ($\mathbf{k}_1$) and (*c*) ($\mathbf{k}_4$) as well as between (*b*) ($\mathbf{k}_2$) and (*d*) ($\mathbf{k}_3$); (*a*) and (*b*) as well as (*c*) and (*d*) on the other hand exhibit significant differences in the configurations of the bright patches.

projected atomic configurations in a one-unit-cell-thick slab. Representative parts of such optical gratings are reproduced in Figs. 10 and 11, whereas the corresponding optical diffraction patterns are shown below each diagram.

In Fig. 10(*a*), the diffraction grating contains exclusively sub-unit-cell elements of the $D1_a$ structure in two variants, whereas in Fig. 10(*b*) only sub-unit-cell atom configurations of the $D0_{22}$ structure are used. The corresponding optical diffraction patterns exhibit maxima which are much broader than those which are actually observed in most electron diffraction patterns. A combination of elements of $D1_a$ and $D0_{22}$ (Fig. 10*c*) leads to a result (Fig. 10*f*) which resembles more closely the electron diffraction pattern. However, the spots in the electron diffraction pattern are still much sharper than those produced by the optical diffraction gratings. This suggests that somewhat larger domains, containing one or a few unit cells, must be assumed.

Fig. 11(*a*) represents an optical grating which contains microdomains of $D0_{22}$ structure of the two orientation variants which have their *c* axis perpendicular to the viewing directions. The atom columns of the third variant all have the same chemical composition and project on f.c.c. sites; they do not contribute to the SRO spots. We have therefore omitted this variant from the model. It is clear that the optical diffraction pattern closely resembles the $1\frac{1}{2}0$ intensity distribution, suggesting that the SRO state consists primarily of microdomains of the $D0_{22}$ structure. In Fig. 11(*b*), APB's having the $D1_a$ configuration have been inserted; the optical diffraction pattern is found to develop 'wings' towards the $D1_a$ spots. In Fig. 11(*c*), finally, more slabs of $D1_a$ structure have been inserted in the (101) rows of the $D0_{22}$ structure. The $D1_a$ spots become already weakly visible, next to the SRO spots in the diffraction pattern of Fig. 11(*f*).

These optical simulation experiments confirm the conclusions derived from the diffraction patterns and from the high-resolution images.

3.4. *SRO coefficients*

Careful measurements of the SRO coefficients for Ni_4Mo, using the diffuse X-ray intensity distribution around the $1\frac{1}{2}0$ positions, have been performed by several authors (Spruiell & Stansbury, 1965; Chakravarti, Starke, Sparks & Williams, 1974). Computer-generated models based on such measurements have been presented by Chakravarti *et al.* (1974). We shall now show that the resulting measured SRO coefficients are compatible with our model. Furthermore, we shall demonstrate also that their computer-generated model is in agreement with our domain models.

The measured SRO coefficients in the alloy, ordered for 5 min at 923 K, obey the following inequalities as to their magnitudes (Spruiell & Stansbury, 1965; Chakravarti *et al.*, 1974):

$$\alpha_{400} > \alpha_{211} > \alpha_{200};$$

we have only considered the three largest positive SRO coefficients, α, which describe the essential features of the structure. The same succession of magnitudes for the largest SRO coefficients is found

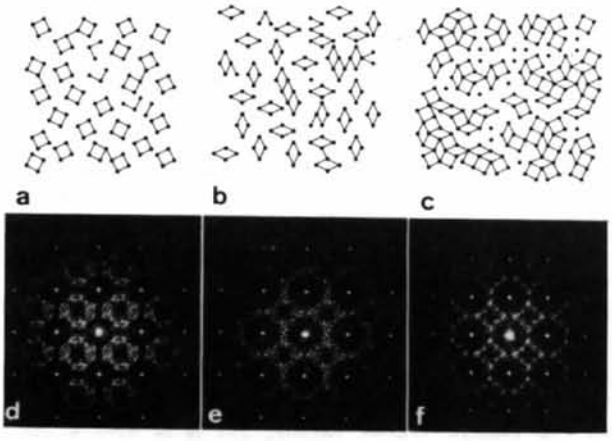

Fig. 10. Three models for optical gratings consisting of: (*a*) only square ($D1_a$) type atom configurations on a cubic lattice; (*b*) only lozenge-shaped ($D0_{22}$) atom configurations on a cubic lattice; (*c*) a mixture of both types of configurations. The lines on the drawings have been added to visualize the arrangements but were not present on the original gratings. (*d*), (*e*), (*f*) Corresponding optical diffraction patterns showing, apart from the cubic lattice, different configurations of diffuse intensity contours.

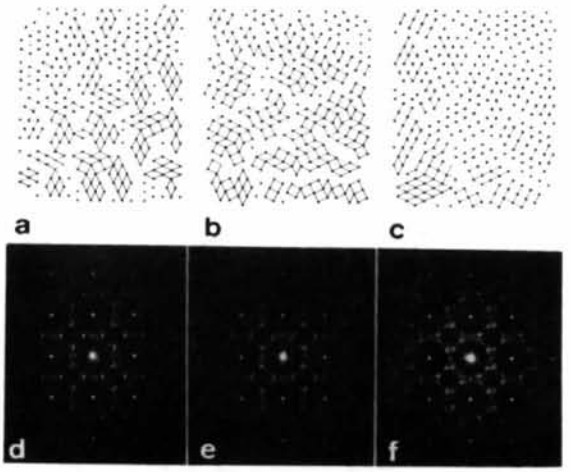

Fig. 11. (*a*), (*b*), (*c*) Models for optical gratings and corresponding optical diffractograms. (*d*), (*e*), (*f*) Illustrating the evolution from SRO towards LRO. (*a*), (*d*) Only $D0_{22}$ fragments separated by single rows of $D1_a$ are used. (*b*), (*e*) $D0_{22}$ as well as $D1_a$ fragments are present. (*c*), (*f*) Mainly $D1_a$ and occasional $D0_{22}$ microdomains are represented. In all cases the *c* domains were omitted; their presence would only lead to a 110 spot, as observed in Fig. 5.

in all of our models. The measured values are, of course, somewhat different for the different models of Fig. 11, but, in all cases, the order of the sequence is the same. On measuring the SRO coefficients on our projected models, we have assumed that the gratings represent a slab one f.c.c. unit cell thick and that the values obtained from such a slab are representative of the whole specimen.

Chakravarti *et al.* (1974) have presented five successive (001) layers of two computer-generated models, based on the experimentally determined SRO coefficients, in the 'as-quenched' state and after a short anneal at 923 K. The authors concluded from these that there was a predominant occurrence of rod-like arrangements of Mo atoms along ⟨100⟩ directions. As the alloy is slightly annealed and becomes more ordered, still remaining in the $1\frac{1}{2}0$ state, the rods appear to become longer. This is also consistent with our observations; unfortunately, the authors failed to represent their results in space. On doing this for layers (1) and (2) of their model (Fig. 12), we find that their Mo arrangements consist, in fact, predominantly of elements of the $D0_{22}$ structure and some elements of the $D1_a$ structure. We have constructed an optical grating based on this computer-generated model by considering again atoms in a slab one f.c.c. unit cell thick. The grating was obtained by superposing layers (1) and (2) and layers (3) and (4) of their Fig. 8 and layers (1) and (2) and layers (3) and (4) of their Fig. 9. The four so-obtained projections were juxtaposed so as to obtain a single sufficiently large grating, which contains a mixture of regions representative of the 'as-quenched' and of the very briefly annealed state (5 min at 923 K). This grating produces an optical diffraction pattern which is similar to the ones produced by our model gratings. It is thus clear that our results are in fact compatible with those obtained by Chakravarti *et al.* (1974), although the authors interpret them quite differently.

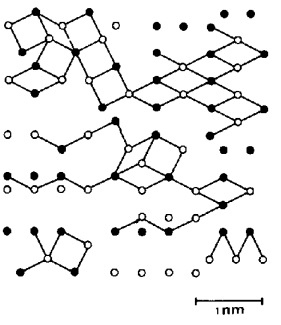

Fig. 12. Structural representation of two successive (001) layers in short-range-ordered Ni_4Mo according to a comptuter-generated model of Chakravarti *et al.* 1974). Open and closed circles represent Mo atoms at two different levels. Ni atoms have been omitted. Note the presence of fragments of $D0_{22}$ structure and elements of $D1_a$ structure.

3.5. *Radiation behavior: equilibrium SRO state*

It is of some interest to discuss the implications of our results on the observations of the radiation behavior of Ni_4Mo. The ordering and disordering of this material under irradiation with 1 MeV electrons was studied by Van Tendeloo & Amelinckx (1981*b*) and by Banerjee, Urban & Wilkens (1984). It was found that, when irradiating in the temperature range 200 to 450 K, an initially long-range-ordered specimen first becomes disordered and subsequently the short-range-ordered state is formed. Irradiation above 450 K always leads to the formation of LRO, unless LRO was destroyed previously by pre-irradiation at a temperature below 200 K; in that case SRO can be developed also by irradiation at 450 K. A surprising conclusion from these observations is that a direct transition from 'SRO' (*i.e.* $1\frac{1}{2}0$ state) to LRO or from LRO to SRO seems to be forbidden in irradiation in the temperature range 220 to 550 K. The fully disordered state must first be formed before the transition is possible. This remarkable result is difficult to understand if the SRO state is merely a prefiguration of the LRO state. However, if the SRO state is a microdomain state based on a structure (in this case $D0_{22}$) different from the LRO state ($D1_a$), it becomes quite understandable that one structure must first be sufficiently disordered before another one can start to form.

On thermal treatment, the behavior is quite different. On annealing at temperatures below the critical temperature for LRO (T_c), an SRO specimen, obtained by quenching from above T_c, transforms into the long-range-ordered state, and it remains in that state on prolonged annealing at that or at a lower temperature. We have also verified whether or not the $1\frac{1}{2}0$ state is the equilibrium SRO state in A_4B alloys. We have performed an experiment on Au_4Cr, where T_c is as low as 603 K: on heating an initially LRO specimen in the electron microscope to just above T_c, the LRO spots rapidly disappear at 613 ± 10 K and the typical SRO pattern of Fig. 13 appears above this temperature. This is in agreement with the results of a similar experiment on Au_3Cr (Das, Okamoto, Fisher & Thomas, 1973). It is thus clear that the $1\frac{1}{2}0$ state is an equilibrium state, just above T_c. At this temperature, $1\frac{1}{2}0$ spots are more diffuse and weaker than in the room-temperature quenched specimens; this is undoubtedly, at least in part, due to the Debye–Waller factor, but it is also a consequence of spinodal ordering which sharpens and intensifies the $1\frac{1}{2}0$ spots as the specimen is cooled below the instability temperature.

These experiments seem to confirm that the quenched-in $1\frac{1}{2}0$ state in Au_4Cr, and presumably also in the other A_4B alloys (except perhaps Au_4Mn), represents the equilibrium SRO state, apart from a possible difference in microdomain size.

4. Discussion

In discussing short-range order, it is important to specify exactly what is meant by that term. Consider first equilibrium states: above the transition temperature, the stable solid solution will contain dynamic equilibrium fluctuations, which may, in fact, be rather intense as a second-order transition or ordering instability is approached. The state just described is that of *equilibrium SRO* proper. The ground state of order at very low temperature is that of *equilibrium LRO*. As explained in § 1, the former state is that which minimizes the second derivative F''; the latter is that which minimizes the internal energy E. Between these two equilibria lies, in principle, a non-denumerable infinity of non-equilibrium states of partial order. For these transition states, it is not really meaningful to ask at what point SRO gives way to LRO; simple descriptions of such states are not available, theories are virtually non-existent. Indeed, there exist no universal minimization procedures which will yield correct evolutionary paths that a system must follow on its way from equilibrium SRO to LRO.

It is precisely these transition states which are really observed by the type of experiments described above; small wonder that clear structural understanding is still lacking. High-temperature equilibrium SRO is best described in reciprocal space, for instance by the Krivoglaz–Clapp–Moss formula. Low-temperature LRO is, of course, most conveniently described in direct space by specifying the unit cell of the ordered structure. In between it is a matter of taste whether one adopts a reciprocal- or a direct-space formulation.

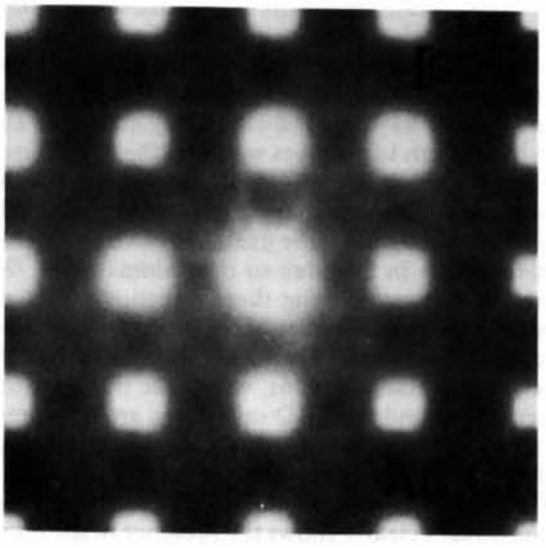

Fig. 13. A [001] electron diffraction pattern of long-range-ordered Au_4Cr heated in the electron microscope just above T_c. Note the disappearance of the LRO reflections, and the presence of weak $1\frac{1}{2}0$ spots. The pattern was recorded at 643 (10) K.

At best, we can try to understand qualitatively the evolution from SRO to LRO: when the solid solution is quenched rapidly from a high temperature, we expect the equilibrium fluctuations to be retained, thereby producing broad, diffuse intensity maxima about the special point (SP) characteristic of that 'family', in the present case, the $1\frac{1}{2}0$ SP. As the ordering spinodal, or the stability limit of the very same SP concentration wave is crossed, the diffuse intensity maxima should intensify, initially in a manner quite independent of the actual average concentration, *i.e.* independent of the final LRO state towards which the system is tending. The reason for this initial independence is that, in the spirit of simple spinodal theory (Cahn, 1961), the early stages of evolution are governed approximately by a linear kinetic equation which 'knows about' F'' only, the latter second derivative containing little information about the final ground state. Soon, however, non-linearities should make their presence felt, and the symmetric diffuse SRO intensity maxima should begin to distort, in a way which will depend on the average concentration, on the type of equilibrium LRO state appropriate for that concentration, on the particular alloy system considered, *i.e.* on the relationship between the various phases present in the phase diagram, and also, as shown for example by Martin (1982), on the type of impurity or third element present. Thus, in the examples considered here, we expect to see different shapes of diffuse intensity patterns in Ni_4Mo, Au_4Cr, Au_4V and Au_4Fe after some amount of 'spinodal ordering' has taken place, although in all four cases both the SP family and the stoichiometry are the same. At present, it is impossible to predict theoretically how the 'intensity transfer' from SRO to LRO will take place.

All we know is that, in intermediate states of order, information about final states must be present in some embryonic way. It is, therefore, tempting to construct simple models combining clusters of atoms in the correct LRO relationship (the $D1_a$ structure in the present case), in various allowed orientations, along with clusters characteristic of the ordered structure closest to the disappearing SRO state (the $D0_{22}$ in the present case). Such 'cluster' models have been constructed in the form of two-dimensional optical diffraction masks (Figs. 10, 11). Similarly two-dimensional mixtures of 'Ni_4Mo'-, 'Ni_3Mo'- and 'Ni_2Mo'-type domains have recently beeen proposed to explain diffuse neutron intensity patterns obtained from PdH and PdD samples at very low temperatures (Blaschko, Fratzl & Klemenic, 1981). Apparently, this hydride system also belongs to the $1\frac{1}{2}0$ family.

It can easily be verified that the cluster relation derived by De Ridder, Van Tendeloo, Van Dyck & Amelinckx (1976) is satisfied at all lattice sites of the $D0_{22}$ structure as well as in the $D1_a$ structure. The linear arrangement of such clusters in bipyramids

along cube directions is a predominant feature of the ideal $D0_{22}$ structure. It thus also turns out that the results of the clusters theory are compatible with the present model, whereby a dominant role is attributed to the $D0_{22}$ structure.

One central question in this discussion is 'do we see microdomains and clusters or not?' In other words, can the bright dots observed in Figs. 6, 7 and 8 be interpreted as minority-atom strings lined up along the electron beam, *i.e.* along one of the cubic axes?

When talking about microdomains with respect to ordering, one usually refers to domains the size of a few unit cells having the long-range-ordered structure. The ordered clusters we possibly observe here by HREM quite often consist only of a small number of bright dots (*i.e.* sometimes less than one unit cell) but extend probably over a few nm along the cube direction perpendicular to it. This conviction is substantiated by the following arguments: if certain atom columns, having the configuration of the minority-atom columns in the LRO structure, are clearly differentiated from the surrounding ones, this can only mean that they also contain almost exclusively minority atoms. Moreover, these columns have to be extended over a sufficient length in order to be sufficiently different from columns containing both types of atoms in the macroscopic proportion.

We will first try to rule out the presence of possible artifacts. One might argue that electropolishing introduces a surface layer which gives rise to moiré-type artifacts or that oxides may be formed at the surface. However, in that case, one would have to assume that Au_4Cr forms a surface layer and, with the same electropolishing solution, Au_4V will not; Ni_4Mo and Au_4Cr would both suffer from it although prepared with a different solution. Moreover, a possible surface layer, which has a constant thickness, would be better observable in thinner areas, which is not the case.

Another argument is that one might actually be looking at the initial stages of LRO rather than at the SRO state. This would be quite possible for Ni_4Mo where fast water quench has been used and a slight anneal of a few seconds at 1073 K already produces long-range-ordering effects observable in the diffraction pattern. However, for Au_4Cr, where the ordering temperature is only about 603 K, the kinetics are very slow and anneals up to 3 h at 543 K did not produce any further ordering effects. Only after anneals of more than 10 h, do long-range-order reflections appear weakly (Dutkiewicz & Thomas, 1975), which denies the probability that any long-range ordering would have taken place during quench in this material.

A striking and interesting feature is that 'microdomains' are not visible close to the edge of the specimen when imaging with the objective diaphragm including f.c.c. reflections while the same area imaged with only the transmitted beam and the eight SRO reflections does show microdomain contrast up to the edge of the specimen (Fig. 6). However, this is not so suprising since similar effects have been observed for long-range-ordered alloys. In the thinnest areas, only the matrix is imaged and, in order to see the ordering effects, one needs a minimum thickness since the structure factor for the ordering reflections is much smaller than the structure factor for the basic reflections. This has been pointed out by Shindo (1982) for ordering in Au-Cd alloys and by Van Dyck, Van Tendeloo & Amelinckx (1982) for the Au-Mn system.

In our model, we have to assume that, at least for some microdomains, the coherency is rather good along the electron beam; *i.e.* the microdomains extend several unit cells along this cube orientation. If this were not the case, one would fail to observe the clusters or dot patterns for two reasons:

(*a*) If the microdomains only extend over 1 or 2 f.c.c. unit cells for a specimen thickness of at least 10 unit cells (*i.e.* 4 nm), one would not observe such pronounced effects.

(*b*) For thin microdomains, one would, of course, have overlapping domains along the imaging direction and, even for a microdomain thick enough to produce a contrast effect, the overall effect would be partly cancelled out due to overlap. The observed dot patterns will then underestimate the order present.

In some cases, one might still observe 'coincidence patterns' under these conditions; these would consist of dot patterns with a geometry that differs from that of the projected structure of a single domain (Van Tendeloo & Amelinckx, 1978).

Assuming extended elongated microclusters along one of the cube orientations, we must have three orientation variants having their *c* axis along all three cube axes. However, with the present HREM techniques, we can only image a fraction of these clusters, namely those having good coherency along the electron beam. This idea agrees well with the X-ray results of Chakravarti *et al.* (1974) who proposed for Ni_4Mo that the first ordering effect is to form extended Mo–Mo chains along the cube axes. We have shown here that these are in fact due to microdomains of $D0_{22}$ structure elongated along these directions. It is also consistent with the further ordering data obtained by electron diffraction by De Ridder, Van Tendeloo, Van Dyck & Amelinckx (1976), where the diffuse circles observed around the SRO reflections are interpreted as being due to pyramidal clusters, which also imply ordering along the cube directions.

Optical diffraction from the observed high-resolution images clearly shows the presence of the diffuse SRO reflections and no presence of any LRO intensity, indicating that at least some information on the SRO state has been recorded in the images. In order to find out the validity of a microdomain

model partly consisting of $D0_{22}$ configurations (lozenges) and partly consisting of $D1_a$ configurations (squares), we produced two-dimensional optical masks for different types of domains (Figs. 10, 11).

It might seem unrealistic to include $D0_{22}$ fragments (AB_3 composition) in the ordering process of AB_4 alloys; however, the $D0_{22}$ structure is the only one, apart from the *AABB* phase with composition *AB* (Khatchaturyan, 1973), having superstructure reflections at the $\langle 1\frac{1}{2}0\rangle$ special points. Moreover, in similar systems (*e.g.* Au–Mn), the $D0_{22}$ structure plays an important role in the ordering process of Au_4Mn (Van Tendeloo, De Ridder & Amelinckx, 1978) as well as in equilibrium $Au_{4-x}Mn$ phases (Van Tendeloo & Amelinckx, 1981*a*; Terasaki, Watanabe, Hiraga, Shindo & Hirabayashi, 1980; Hiraga, Shindo, Hirabayashi, Terasaki & Watanabe, 1980; Hiraga, Hirabayashi, Terasaki & Watanabe, 1982). This is summarized in Fig. 14 where the three Au–Mn equilibrium phases between 20 and 23% Mn are reproduced under high-resolution conditions (upper part) and in a schematic representation (lower part), where only the Mn configurations are indicated. Close to Au_4Mn one forms a one-dimensional (Fig. 14*a*) and a two-dimensional long-period superstructure (Fig. 14*b*) of Au_4Mn. Along the boundaries, a $D0_{22}$ configuration (triangular arrangement of bright dots) results. At 23% Mn, the basic structure is $D0_{22}$ but with two-dimensional periodic antiphase boundaries along which the $D1_a$ configuration (square arrangement) is retained. This phase, although ideally not having the A_4B composition, occurs invariably as a high-temperature transition structure during the ordering process of perfectly stoichiometric Au_4Mn (Van Tendeloo, De Ridder & Amelinckx, 1978).

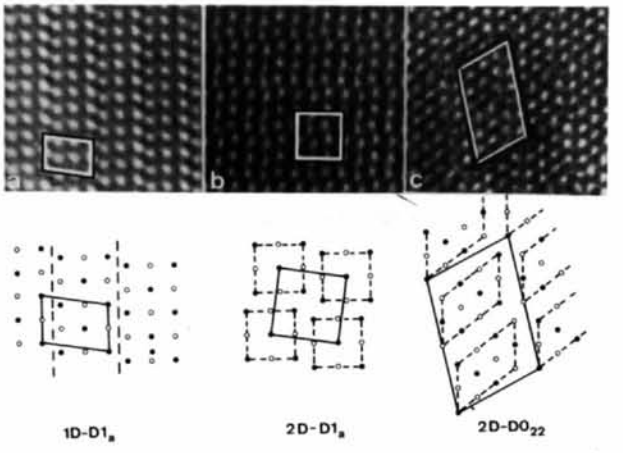

Fig. 14. High-resolution images (upper part) as well as schematic representations (lower part) of three structures intermediate between A_4B ($D1_a$) and A_3B ($D0_{22}$) in the Au–Mn system. (*a*) A one-dimensional long-period structure of the $D1_a$ phase (1D-$D1_a$). (*b*) A two-dimensional long-period structure of $D1_a$ (2D-$D1_a$). (*c*) A two-dimensional long-period structure based on the $D0_{22}$ structure (2D-$D0_{22}$). In the $D1_a$-based phases (*a* and *b*) the $D0_{22}$ configuration is locally formed along the interfaces; in $D0_{22}$-based structures (*c*) $D1_a$ is formed along the interfaces.

A transmission-electron-microscopy foil, though very thin, is a three-dimensional object. Enlarging somewhat on the proposed model, we may then regard the thin foil as made up of several stacked layers of two-dimensional patterns, similar to the ones described above, bearing a certain degree of positional or orientational relationship to one another. Because of this partially random stacking, the projection of the resulting structure will only occasionally reveal the original $D1_a$ or $D0_{22}$ clusters. Hence, the projected image will tend to exhibit islands of ordered domains in a sea of disordered material, as may be seen, for instance, in the micrographs of Figs. 6 and 7. Such an artificial interpretation would result from the fact that, in an electron micrograph, one does not see three-dimensional space, but a two-dimensional projection thereof; it would underestimate the order present.

To the question 'does high-resolution TEM reveal microdomains?' one may tentatively answer: 'One sees apparently ordered microdomains wherever clusters, characteristic of transition states intermediate between equilibrium SRO and LRO, happen to project coherently'. It is quite clear that there is more order than revealed in this way by the high-resolution images due to the overlap effects.

Work on Au–Fe was performed at the National Center for Electron Microscopy by Dr W. M. Stobbs of Cambridge University. Samples were provided by Drs R. J. Borg and C. Violet of the Lawrence Livermore Laboratory, and sample preparation was performed by Mr M. Eberhard. A portion of this work, which was carried out at Lawrence Berkeley Laboratory, was supported by the Director, Office of Energy Research, Office of Basic Energy Sciences, Materials Sciences Division of the US Department of Energy under contract No. DE-AC03-76SF00098.

References

BANERJEE, S., URBAN, K. & WILKENS, M. (1984). *Acta Metall.* **32**, 299–311.

BLASCHKO, O., FRATZL, P. & KLEMENIC, R. (1981). *Phys. Rev. B*, **24**, 277–282.

CAHN, J. W. (1961). *Acta Metall.* **9**, 795–801.

CHAKRAVARTI, B., STARKE, E. A. JR, SPARKS, C. S. J. & WILLIAMS, R. O. (1974). *J. Phys. Chem. Solids*, **35**, 1317–1326.

CHEVALIER, J. P. A. A. (1980). *J. Microsc.* **119**, 113–124.

CHEVALIER, J. P. A. A. & STOBBS, W. M. (1979). *Acta Metall.* **27**, 1197–1217.

DARTYGE, E., BOUCHIAT, H. & MONOD, P. (1982). *Phys. Rev. B*, **25**, 6995–7002.

DAS, S. K., OKAMOTO, P. R., FISHER, P. & THOMAS, G. (1973). *Acta Metall.* **21**, 913–928.

DE RIDDER, R., VAN TENDELOO, G. & AMELINCKX, S. (1976). *Acta Cryst.* A**32**, 216–224.

DE RIDDER, R., VAN TENDELOO, G., VAN DYCK, D. & AMELINCKX, S. (1976). *Phys. Status Solidi A*, **38**, 663–674.

DUTKIEWICZ, J. & THOMAS, G. (1975). *Metall. Trans.* **6A**, 1919-1928.
FONTAINE, D. DE (1975). *Acta Metall.* **23**, 553-571.
FONTAINE, D. DE (1979). *Solid State Phys.* **34**, 73-274.
FURNROHR, P. (1976). PhD Thesis, Univ. of Stuttgart.
HIRAGA, K., HIRABAYASHI, M., TERASAKI, O. & WATANABE, D. (1982). *Acta Cryst.* A**38**, 269-274.
HIRAGA, K., SHINDO, D., HIRABAYASHI, M., TERASAKI, O. & WATANABE, D. (1980). *Acta Cryst.* B**36**, 2550-2554.
KESTERNICH, W., CARPENTER, R. W. & KENIK, E. A. (1982). *Metall. Trans.* **13A**, 213-219.
KHATCHATURYAN, A. G. (1973). *Phys. Status Solidi B*, **60**, 9-37.
MARTIN, P. L. (1982). PhD Thesis, Carnegie-Mellon Univ.
OKAMOTO, P. R. & THOMAS, G. (1971). *Acta Metall.* **19**, 825-841.
RUEDL, E., DELAVIGNETTE, P. & AMELINCKX, S. (1968). *Phys. Status Solidi*, **28**, 305-328.
SHINDO, D. (1982). *Acta Cryst.* A**38**, 310-317.
SPRUIELL, J. E. & STANSBURY, E. E. (1965). *J. Phys. Chem. Solids*, **26**, 811-822.
STOBBS, W. M. (1983). Private communication.
STOBBS, W. M. & CHEVALIER, J. P. A. A. (1978). *Acta Metall.* **26**, 233-240.
TERASAKI, O., WATANABE, D., HIRAGA, K., SHINDO, D. & HIRABAYASHI, M. (1980). *Micron*, **11**, 235-240.
THOMAS, G. & SINCLAIR, R. (1977). *Acta Metall.* **25**, 231-234.
VAN DYCK, D., VAN TENDELOO, G. & AMELINCKX, S. (1982). *Ultramicroscopy*, **10**, 263-280.
VAN TENDELOO, G. (1976). *Mater. Sci. Eng.* **26**, 209-220.
VAN TENDELOO, G. (1980). *J. Microsc.* **119**, 125-140.
VAN TENDELOO, G. & AMELINCKX, S. (1978). *Phys. Status Solidi A*, **47**, 555-564.
VAN TENDELOO, G. & AMELINCKX, S. (1981*a*). *Phys. Status Solidi A*, **65**, 73-86, 431-446.
VAN TENDELOO, G. & AMELINCKX, S. (1981*b*). *J. Microsc. Spectrosc.* **6**, 371-382.
VAN TENDELOO, G. & AMELINCKX, S. (1983). *Phys. Status Solidi A*, **77**, K9-K11.
VAN TENDELOO, G., DE RIDDER, R. & AMELINCKX, S. (1978). *Phys. Status Solidi A*, **49**, 655-666.

Acta Cryst. (1985). B**41**, 292-298

An Investigation of a Metastable Form of GaS by Convergent-Beam Electron Diffraction and High-Resolution Electron Microscopy

BY P. GOODMAN, A. OLSEN* AND H. J. WHITFIELD

Division of Chemical Physics, CSIRO, Melbourne, Australia

(*Received* 27 *December* 1983; *accepted* 9 *April* 1985)

Abstract

GaS prepared at temperatures below that required for adequate annealing is found to yield microcrystals with a much higher stacking-fault density and correspondingly lower overall crystal symmetry than that found for hexagonal β-GaS. The results of a high-resolution electron-microscopy analysis suggest that this character is associated with the predominance in the material of a high-pressure modification of GaS, present metastably in the partially annealed sample. It is concluded that details of preparation, including final annealing, are important in determining the microscopic crystal structure, and that discrepancies which have been highlighted recently between single-crystal diffraction measurements and those carried out on bulk microcrystalline samples may largely be explained by differences in preparative technique.

I. Introduction

Convergent-beam electron diffraction has in the past been largely used for examination of highly perfect crystal regions, and its application to structural study of faulted materials has been relatively little exploited. The earlier analysis of β-GaS (Goodman & Whitfield, 1980) is a good example of CBED analysis of fault-free single-crystal regions. This phase is formed by high-temperature annealing, above 1173 K, and the macrocrystals are in the form of graphite-like sheets, with a ready micaceous cleavage.

However, several alternative methods have been used in preparing GaS for analysis, particularly when finely powdered samples are required, including one in which the annealing is carried out below 973 K. Material prepared in this way has been recently examined by Bastow, Campbell & Whitfield (1981) using nuclear quadrupole resonance (NQR). Their finding of a new characteristic NQR spectrum has added to the already considerable debate about the nature of structural variants occurring at room temperature and pressure. Since crystals from this preparation are characteristically too small for single-crystal X-ray diffraction, this appeared as an ideal project for joint study by CBED and high-resolution electron microscopy. A brief summary of previous investigation is given below.

* Permanent address: Department of Physics, University of Oslo, Norway.

0108-7681/85/050292-07$01.50